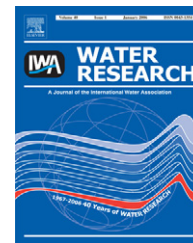


Available at www.sciencedirect.comjournal homepage: www.elsevier.com/locate/watres

Coupling of physical and chemical mechanisms of colloid straining in saturated porous media

Scott A. Bradford^{a,*}, Saeed Torkzaban^b, Sharon L. Walker^b

^aUS Salinity Laboratory, USDA-ARS, 450 W. Big Springs Road, Riverside, CA 92507-4617, USA

^bDepartment of Chemical and Environmental Engineering, University of California, Riverside, CA 92521, USA

ARTICLE INFO

Article history:

Received 30 November 2006

Received in revised form

2 February 2007

Accepted 20 March 2007

Available online 2 May 2007

Keywords:

Colloid

Transport

Straining

Attachment

Filtration theory

Modeling

ABSTRACT

Filtration theory does not include the potential influence of pore structure on colloid removal by straining. Conversely, previous research on straining has not considered the possible influence of chemical interactions. Experimental and theoretical studies were therefore undertaken to explore the coupling of physical and chemical mechanisms of colloid straining under unfavorable attachment conditions (pH = 10). Negatively charged latex microspheres (1.1 and 3 μm) and quartz sands (360, 240, and 150 μm) were used in packed column studies that encompassed a range in suspension ionic strengths (6–106 mM) and Darcy water velocities (0.1–0.45 cm min^{-1}). Derjaguin–Landau–Verwey–Overbeek (DLVO) calculations and torque analysis suggests that attachment of colloids to the solid–water interface was not a significant mechanism of deposition for the selected experimental conditions. Effluent concentration curves and hyperexponential deposition profiles were strongly dependent on the solution chemistry, the system hydrodynamics, and the colloid and collector grain size, with greater deposition occurring for increasing ionic strength, lower flow rates, and larger ratios of the colloid to the median grain diameter. Increasing the solution ionic strength is believed to increase the force and number of colloids in the secondary minimum of the DLVO interaction energy profile. These weakly associated colloids can be funneled to small regions of the pore space formed adjacent to grain–grain junctions. For select systems, the ionic strength of the eluant solution was decreased to 6 mM following the recovery of the effluent concentration curve. In this case, only a small portion of the deposited colloids was recovered in the effluent and the majority was still retained in the sand. These observations suggest that the extent of colloid removal by straining is strongly coupled to solution chemistry.

© 2007 Elsevier Ltd. All rights reserved.

1. Introduction

Considerable research has been devoted to the fate and transport of microbes (biocolloids) and colloids in porous media (reviews are given by Schijven and Hassanizadeh, 2000; Harvey and Harms, 2002; Jin and Flury, 2002; Ginn et al., 2002). The bulk of existing colloid literature considers deposition to be controlled by attachment of colloids on grain surfaces.

Mass transfer of colloids to the solid–water interface occurs via diffusion, interception, and sedimentation (Yao et al., 1971). Attachment involves collision with and subsequent retention of colloids at the solid–water interface. Once a colloid approaches the solid–water interface, attachment depends on a combination of forces and/or torques that act on the colloid (Cushing and Lawler, 1998; Bergendahl and Grasso, 1998; Li et al., 2005) at this location. These forces

*Corresponding author. Tel.: +1 951 369 4857; fax: +1 951 342 4963

E-mail address: sbradford@ussl.ars.usda.gov (S.A. Bradford).

0043-1354/\$ - see front matter © 2007 Elsevier Ltd. All rights reserved.

doi:10.1016/j.watres.2007.03.030

include gravity and buoyancy, hydrodynamic drag and lift, electrical double-layer repulsion (or attraction), and London–van der Waals interaction.

In the presence of an energy barrier (unfavorable attachment conditions) the transport and deposition behavior of colloids is frequently found to be inconsistent with clean bed filtration theory (CFT) predictions (Albinger et al., 1994; Camesano and Logan, 1998; Bolster et al., 1999; Redman et al., 2001; Bradford et al., 2002; Tufenkji et al., 2003; Li et al., 2004; Tong et al., 2005; Li and Johnson, 2005; Tufenkji and Elimelech, 2005a,b). Specifically, the deposition coefficient has commonly been observed to exhibit a depth dependence and the concentration of retained colloids do not decrease exponentially with distance as CFT would predict. Deviation between CFT predictions and experimental data has been reported to be increasingly significant for larger colloids and finer textured porous media (Bradford et al., 2002; Tufenkji and Elimelech, 2005a). Bradford et al. (2003) reported that filtration theory predictions no longer adequately describe the measured deposition profiles when the ratio of the colloid diameter to the median grain diameter is greater than around 0.005.

Filtration theory assumes a model collector (such as Happel's sphere-in-cell model which is an isolated collector in an assemblage of collectors) that neglects the actual pore structure and pores formed by grain–grain contacts which occur in porous media. However, recent experimental and theoretical research has indicated that the pore structure can play an important role in colloid deposition under unfavorable attachment conditions (Cushing and Lawler, 1998; Bradford et al., 2002, 2003, 2004, 2005, 2006a–d; Li et al., 2004, 2006a,b; Tufenkji et al., 2004; Bradford and Bettahar, 2005, 2006; Foppen et al., 2005). This removal likely occurs by straining, which is the retention of colloids in the smallest regions of the soil pore space formed adjacent to points of grain–grain contact (Cushing and Lawler, 1998). Pore spaces occurring at grain contacts provide optimum locations for colloids that are weakly associated with the solid phase (secondary energy minima) to be retained because of reduced hydrodynamic forces, pore size limitations, and enhanced Derjaguin–Landau–Verwey–Overbeek (DLVO) interactions (Hoek and Agarwal, 2006).

Most published research on straining has focused on the role of physical factors such as the relative size of the colloid and porous medium, and little attention has been given to the potential interrelated influence of solution chemistry and hydrodynamics on straining. Attachment under unfavorable conditions is known to be highly dependent on solution chemistry (e.g., Li et al., 2004; Tufenkji and Elimelech, 2004, 2005a), and system hydrodynamics (Wang et al., 1981; Tan et al., 1994; Kretzschmar et al., 1997; Compere et al., 2001; Li et al., 2005). Under such attachment conditions, hydrodynamic forces may be sufficient to overcome the weak association of colloids in the secondary energy minimum of the DLVO interaction energy distribution (Kuznar and Elimelech, 2007). In this case, attached colloids may be lifted from the solid surface and detach, or they may roll or slide down gradient on the grain surface to locations where the hydrodynamic shear is less significant. Bergendahl and Grasso (1998) demonstrated that rolling is often the primary mechanisms for hydrodynamic

motion of detached colloids. It is logical to anticipate that some of the colloids rolling on the grain surface may be retained in straining locations (i.e., smallest regions of the pore space formed at grain–grain contact points). One can therefore expect that solution chemistry and hydrodynamic forces will play an important interrelated role in straining.

The objective of this research is to investigate the role of solution chemistry and system hydrodynamics on colloid transport and straining. Negatively charged latex microspheres and quartz sands were used in packed column studies that encompassed a range of solution IS (6–106 mM) and Darcy water velocity (0.1–0.45 cm min⁻¹). All experiments were conducted using electrolyte solution buffered to a pH of 10 to ensure highly unfavorable attachment conditions. Data analysis and interpretation was aided through DLVO calculations of the total interaction energy between the colloids and quartz surfaces, analysis of torques, mass balance computation, and experimental effluent concentration curves and deposition profiles.

2. Material and methods

2.1. Colloids

Yellow–green fluorescent latex microspheres (Molecular Probes, Eugene, OR) were used as model colloid particles in the experimental studies (excitation at 505 nm, and emission at 515 nm). Two sizes of microspheres were used in the transport experiments, 1.1 and 3.0 μm. The uniformity of the colloid size was verified using a Horiba LA 930 (Horiba Instruments Inc., Irvine, CA) laser scattering particle size and distribution analyzer and by inspections of suspensions under an epi-fluorescent microscope. The microspheres had carboxyl surface functional groups, a density of 1.055 g cm⁻³, and are reported as hydrophilic by the manufacturer. The initial influent concentration (C_i) for the 1.1 and 3.0 μm colloids for the experiments was 2.7×10^{10} and $1.3 \times 10^9 N_c L^{-1}$ (where N_c denotes number of colloids), respectively. Several experiments with the 1.1 μm colloids were also conducted at a lower initial concentration of $C_i = 6.8 \times 10^8 N_c L^{-1}$.

2.2. Sand

Aquifer material used for the column experiments consisted of various sieve sizes of Ottawa sand (US Silica, Ottawa, IL). The porous media were selected to encompass a range in grain sizes, and are designated by their median grain size (d_{50}) as: 360, 240, and 150 μm. Specific properties of the 360, 240, and 150 μm sands include: the coefficient of uniformity (d_{60}/d_{10} ; here 10% and 60% of the sand mass is finer than d_{10} and d_{60} , respectively) of 1.88, 3.06, and 2.25; and intrinsic permeabilities of 6.37×10^{-11} , 1.12×10^{-11} , and $4.68 \times 10^{-12} m^2$, respectively. Ottawa sands typically consist of 99.8% SiO₂ (quartz) and trace amounts of metal oxides, have spheroidal shapes, and contain relatively rough surfaces. An estimate of the pore-size distribution for these sands can be obtained by using Laplace's equation of capillarity and measured capillary pressure–saturation curves presented by Bradford and Abriola (2001).

2.3. Electrolyte solution chemistry

The background electrolyte solutions utilized in the column studies consisted of deionized water with a buffered pH of 10 achieved with 1.7 mM NaHCO₃ and 1.7 mM Na₂CO₃ (Cherrey et al., 2003). This solution chemistry was chosen to create a stabilized mono-dispersed suspension with the selected colloids. In particular, at a pH of 10 quartz and iron oxides possess a net negative charge (Tipping, 1981; Redman et al., 2004), and any attractive electrostatic interactions between the colloids and porous media is expected to be minimized at this pH. The ionic strength (IS) of the eluant, resident, and tracer solutions in the transport experiments was varied using this same pH 10 solution by changing the amounts of added NaCl (eluant and resident solutions) or NaBr (tracer). Unless specifically indicated, the concentrations of NaCl (resident and eluant solutions) and NaBr (tracer) in solution were maintained over the course of an experiment at 6, 31, 56, 81, or 106 mM. On select experiments the IS of the eluant solution was lowered to 6 mM NaCl for an additional 2.1–3.3 pore volumes after recovery of the effluent concentration curve (the first 8–10 pore volumes). All of the colloid tracer solutions consisted of the pH 10 NaBr solution (IS of 6, 31, 56, 81, or 106 mM), and the previously indicated initial colloid concentration.

2.4. Column experiments

Procedures and protocols for the packed column experiments are reported in detail by Bradford et al. (2002). Only an abbreviated discussion is provided below. Kontes Chromaflex chromatography columns (Kimble/Kontes, Vineland, NJ) made of borosilicate glass (15 cm long and 4.8 cm inside diameter) were equipped with an adjustable adapter at the top) were used in the transport studies. The columns were wet packed (water level kept above the sand surface) with the various sands. Table 1 provides porosity (ϵ) values and column length (L_c) for each experimental system. The colloid suspension was pumped upward through the vertically oriented columns at a steady flow rate, after which a three-way valve was used to switch to the background solution. The average Darcy velocities (q) and colloid pulse duration in terms of pore volumes (PV_0) for the various experiments are given in Table 1. Effluent samples were collected and analyzed for colloid concentration using a Turner Quantech Fluorometer (Barnstead/ThermoLyne, Dubuque, IA). The average of three measurements were used to determine each colloid concentration (reproducibility was typically within 1% of C_i).

Following completion of the colloid transport experiments, the spatial distribution of retained colloids in each packed column was determined. The saturated sand was carefully excavated into 50 ml Falcon centrifuge tubes containing excess eluant solution of the same IS and pH that was used in the transport experiment. The tubes were slowly shaken for 15 min using a Eberbach shaker (Eberbach Corporation, Ann Arbor, MI) to liberate reversibly retained colloids. The concentration of the colloids in the excess aqueous solution was measured with the fluorometer, using the same experimental protocol as followed for the effluent samples. The volume of solution and mass of sand in each tube was determined from mass balance.

A colloid mass balance was conducted at the end of each column experiment using effluent concentration data and the final spatial distribution of retained colloids in the sand. The calculated number of colloids in the effluent and retained in the sand was normalized by the total number of injected particles into a column. Table 1 presents the calculated colloid mass percentages that were recovered for all the experiments in the effluent (M_{eff}), sand (M_{sand}), and the total ($M_{total} = M_{eff} + M_{sand}$) system.

2.5. DLVO calculations

DLVO theory (Derjaguin and Landau, 1941; Verwey and Overbeek, 1948) was used to calculate the total interaction energy (sum of London–van der Waals attraction and electrostatic double-layer repulsion) for our 1.1 and 3 μ m colloids upon close approach to quartz surfaces (assuming sphere-plate interactions) for the various solution chemistries (pH = 10, and IS = 6, 31, 56, 81, and 106 mM). In these calculations, constant-potential electrostatic double-layer interactions were quantified using the expression of Hogg et al. (1966) and zeta potentials in place of surface potentials. Retarded London–van der Waals attractive interaction force was determined from the expression of Gregory (1981) utilizing a value of 4.04×10^{-21} J for the Hamaker constant (Bergendahl and Grasso, 1999) to represent our polystyrene latex-water–quartz system. The zeta potential of the quartz at pH 10 and for IS ranging from 6 to 106 mM was estimated using results presented in Elimelech et al. (2000) and Kuznar and Elimelech (2007). Zeta potentials for our 1.1 and 3 μ m colloids in the various solution chemistries that were used in the DLVO calculations were calculated from experimentally measured electrophoretic mobilities using a ZetaPals instrument (Brookhaven Instruments Corporation, Holtsville, NY).

2.6. Applied and resisting torques

Bergendahl and Grasso (1999, 2000) provide a mathematical framework to examine the influence of hydrodynamics on colloid detachment in porous media. These authors found that detachment occurred primarily by rolling when the applied torque from hydrodynamic shear overcame the resistance associated with rolling. Lifting and sliding of attached colloids were much less significant mechanisms of detachment and were therefore not considered herein. The detachment of retained polystyrene colloids in glass beads was well predicted by this model. We utilize this approach to determine the conditions when detachment of colloids retained in the DLVO secondary minimum is likely.

The resisting torque for colloids attached in the DLVO secondary minimum (T_{res} ; ML^2T^{-2} ; M , L , and T denotes units of mass, length, and time, respectively) to fluid flow is given as:

$$T_{res} = a_0 F_{DLVO}, \quad (1)$$

where F_{DLVO} [MLT^{-2}] is the DLVO force of adhesion and a_0 [L] is the contact radius. To obtain F_{DLVO} in terms of interaction energy the Derjaguin and Langbein approximations (Israelachvili, 1992) were employed. Specifically, the value of F_{DLVO}

Table 1 – Column properties (Darcy velocity, q ; porosity, ε ; column length, L_c ; and colloid pulse duration in terms of pore volumes, PV_0) and the effluent (M_{eff}), sand (M_{sand}), and the total (M_{total}) mass percentage recovered for the experimental systems

IS mM	d_c μm	d_{50} μm	q cm min^{-1}	ε —	L_c cm	PV_0 —	M_{eff} %	M_{sand} %	M_{total} %
6	3	360	0.096	0.35	12.9	1.6	60.3	37.2	97.5
6	3	240	0.104	0.32	12.3	2.0	14.3	71.5	85.8
6	3	150	0.096	0.35	12.8	1.6	6.0	84.7	90.7
6	3	360	0.506	0.33	12.5	1.8	38.1	47.5	85.6
6	3	240	0.466	0.33	12.4	1.7	6.4	86.6	93.0
6	3	150	0.463	0.36	13.1	1.5	1.4	86.7	88.1
6	1.1	360	0.107	0.32	12.2	2.1	102.9	3.6	106.5
31	1.1	360	0.107	0.35	12.8	1.8	97.9	22.0	119.9
56	1.1	360	0.099	0.34	12.6	1.7	43.5	39.6	83.1
81	1.1	360	0.085	0.34	12.6	1.5	42.9	60.2	103.1
106	1.1	360	0.101	0.33	12.4	1.9	0.6	89.6	90.2
6	1.1	240	0.089	0.28	11.6	2.1	100.0	4.6	104.6
31	1.1	240	0.093	0.30	12.0	2.2	82.5	13.4	95.9
56	1.1	240	0.104	0.30	12.0	2.2	32.1	53.7	85.8
81	1.1	240	0.092	0.31	12.1	1.8	25.9	79.2	105.1
106	1.1	240	0.098	0.33	12.5	1.8	0	99.5	99.5
6	1.1	150	0.104	0.33	12.5	1.9	94.9	14.2	109.1
31	1.1	150	0.098	0.35	12.8	1.9	86.7	16.1	102.8
56	1.1	150	0.099	0.35	12.8	1.7	21.3	70.3	91.6
81	1.1	150	0.084	0.35	12.9	1.4	16.4	85.6	102.0
106	1.1	150	0.101	0.34	12.7	1.8	0	91.4	91.4
56	1.1	360	0.230	0.34	12.6	2.0	45.4	41.7	87.1
56	1.1	240	0.289	0.35	12.8	2.4	27.2	56.6	83.8
56 [†]	1.1	150	0.229	0.34	12.7	2.0	18.8	62.8	81.6
56	1.1	360	0.479	0.33	12.4	1.8	80.3	18.5	98.8
56	1.1	240	0.411	0.32	12.3	1.6	67.1	43.2	110.3
56 ^b	1.1	150	0.446	0.36	13.0	1.4	52.1	50.0	102.1
56/6 ^a	1.1	360	0.216	0.35	12.8	5.4	46.0	43.1	89.1
56/6 ^a	1.1	240	0.197	0.36	13.1	4.7	32.4	64.3	96.7
56/6 ^{a,b}	1.1	150	0.198	0.35	12.9	4.9	25.1	69.3	94.4
106/6 ^a	1.1	360	0.250	0.33	12.4	6.9	38.7	90.0	128.7
106/6 ^a	1.1	240	0.256	0.32	12.3	7.3	12.3	91.6	104.0
106/6 ^a	1.1	150	0.257	0.35	12.7	6.5	10.7	115.8	126.5
6 ^b	1.1	150	0.215	0.36	13.0	1.7	83.3	7.1	90.4

^a The IS of the colloid suspension and eluting solution was 56 or 106 mM for the first 8.2–12.4 pore volumes, followed by an additional 2.1–3.2 pore volume flush of 6 mM solution.

^b Published in Bradford et al. (2006d).

was estimated as $\Phi_{2\min}^*/d_0$; where $\Phi_{2\min}^*$ [ML^2T^{-2}] is the absolute value of the secondary minimum interaction energy and d_0 [L] is the separation distance between the colloid and the solid surface. The value of a_0 is by given by Li et al. (2005) as

$$a_0 = \left(\frac{4r_c F_{DLVO}}{K_i} \right)^{1/3}, \quad (2)$$

where r_c [L] is the colloid radius and K_i [$\text{ML}^{-1}\text{T}^{-2}$] is the elastic interaction constant. Bergendahl and Grasso (2000) employed a values of $K_i = 4.014 \times 10^9 \text{Nm}^{-2}$ for glass beads and polystyrene colloids and we assume this values for the calculations discussed herein. The above analysis provides a conservative (larger) estimate of T_{res} because colloids attached in the secondary minimum have been treated in an analogous fashion as those in the primary minimum.

The torque applied to attached colloids as a result of the fluid drag force (T_{app} ; ML^2T^{-2}) is given as (Bergendahl and Grasso, 2000)

$$T_{app} = 10.205\pi\mu_w r_c^3 \left(\frac{\partial v}{\partial r} \right), \quad (3)$$

where μ_w [$\text{ML}^{-1}\text{T}^{-1}$] is the water viscosity, and $\partial v/\partial r$ [T^{-1}] is the velocity shear rate that acts on attached colloids. The value of the shear rate can be calculated for simple pore geometries. For example if we consider the porous media as a bundle of capillary tubes of different sizes, then the shear rate (at $R-r_c$; where R [L] is the radius of a given capillary tube) in a given capillary tube can be derived from Poiseuille's Law as

$$\frac{\partial v}{\partial r} = \frac{\Delta P}{2\mu_w L_{ct}} (R - r_c), \quad (4)$$

where ΔP [NL^{-2}] is the pressure difference across the capillary tube, and L_{ct} [L] is the capillary tube length. Eq. (4) indicates that the shear rate is proportional to the capillary tube radius and the pressure gradient. It follows from Eq. (3) that T_{app} is also proportional to these variables. For a given conductivity and Darcy velocity in a porous medium, the value of $\Delta P/L_{ct}$ in Eq. (4) can be estimated using Darcy's Law for horizontal flow. In the experiments discussed herein the value of $\Delta P/L_{ct}$ ranged from 15 696 (360 sand when $q = 0.1 \text{ cm min}^{-1}$) to 961478 (150 sand when $q = 0.45 \text{ cm min}^{-1}$) Nm^{-3} . It should also be mentioned that the maximum velocity and the average water flux in a given sized capillary tube are proportional to the square of the tube radius (e.g., Jury et al., 1991). Hence, for a given pressure gradient higher flow rates and average water fluxes occur through larger than smaller capillary tubes.

3. Results and discussion

3.1. Impact of solution chemistry on colloid retention

Table 1 summarizes experimental conditions and mass balance information for all column experiments. Values of M_{total} typically ranged from 83% to 110%. Three column experiments had values of M_{total} that were somewhat higher (<129%), presumably due to background interference of natural colloids in these sands that impacted values of M_{sand} . Recall that deposition profiles were obtained after excavating the sand from the column, and gently shaking the sand in excess eluant solution of the same solution chemistry that was used in the transport experiment. Values of M_{total} close to 100% in Table 1 therefore indicates that the retained colloids were only weakly associated with the Ottawa sands for the selected solution chemistries. In further support of these findings, Torkzaban et al. (2006) conducted batch experiments with the same 1.1 μm colloids and sands, and similar solution chemistries (up to 60mM) and found negligible sorption of these colloids onto the sand grains, suggesting only minimal association with these surfaces.

Table 2 provides values of zeta potential for the modified carboxyl latex colloids and quartz in the various solution chemistries that were employed in this study. The zeta potential for the colloids was determined directly from measured electrophoretic mobilities, whereas those for the

quartz sands were estimated from published literature (Elimelech et al., 2000; Kuznar and Elimelech, 2007). The zeta potential for the colloids and quartz decreased with increasing IS, but were still highly negatively charged for the selected solution chemistries. Table 2 also provides calculated values of the repulsive energy barrier height (Φ_{max}) and the depth of the secondary minimum ($\Phi_{2min} = \Phi_{2min}^*/k_b T_k$; where k_b is the Boltzmann constant and T_k is the temperature in degrees Kelvin) for the same experimental conditions. For the 1.1 μm colloid, as the IS of the solution was increased the height of the repulsive energy barrier decreased from 5700 to 50 $k_b T_k$ and attachment in the primary minimum is therefore not expected for these conditions. The value of Φ_{2min} also decreased with increasing IS from -0.2 to -7.2 $k_b T_k$, this indicates that the 1.1 μm colloids are only weakly associated with the quartz surface via the secondary energy minimum, even in the highest IS solution examined (106 mM).

Based upon the predictive calculations shown in Table 2, colloid diffusion and hydrodynamic drag forces are likely sufficient to overcome the weak association of colloids in the secondary minimum (e.g., Redman et al., 2004; Walker et al., 2004; Brow et al., 2005). Calculated applied and resisting torques for colloid detachment provide further support for this hypothesis. Table 2 gives values of T_{res} for the various solution chemistry and colloids considered herein, whereas Table 3 shows values of T_{app} for 1.1 and 3 μm colloids in several different sized capillary tubes (ranging in radius from 100 to 2.5 μm) at the minimum ($\Delta P/L_{ct} = 156\,96 \text{ Nm}^{-3}$ for the 360 sand when $q = 0.1 \text{ cm min}^{-1}$) and maximum ($\Delta P/L_{ct} = 961\,478 \text{ Nm}^{-3}$ for 150 sand when $q = 0.45 \text{ cm min}^{-1}$) value of the pressure gradient that was achieved in our column experiments. The value of T_{app} decreased as the radius of the capillary decreased and the size of the colloid decreased, and increased with increasing velocity (pressure gradient). Comparison of values for T_{res} (Table 2) and T_{app} (Table 3) indicate that T_{res} is always less than T_{app} (by several orders of magnitude). Colloid detachment will occur via rolling when $T_{app} > T_{res}$, hence, these values predict that colloid detachment will always occur for our experimental conditions. The above analysis, however, does not consider the potential influence of pore and colloid size limitations on colloid retention. Colloids that interact with the solid phase can still be retained, if they roll along the surface of the solid

Table 2 – Total interaction energy parameters (energy barrier, Φ_{max} ; and secondary minima, Φ_{2min}) obtained from DLVO calculations for planar quartz surfaces and latex microspheres for experimental solution chemistries (see Section 2 in text for details of the calculations)

d_c (μm)	IS (mM)	ζ_c (mV)	ζ_g (mV)	Φ_{max} ($k_b T_k$)	Φ_{2min} ($k_b T_k$)	T_{res} (Nm)
1.1	6	-104	-80	5700	-0.2	3.4E-24
1.1	31	-104	-30	940	-1.4	2.1E-22
1.1	56	-104	-20	400	-2.8	8.5E-22
1.1	81	-78	-15	180	-4.6	2.8E-21
1.1	106	-64	-10	50	-7.2	7.8E-21
3.0	6	-76	-80	12000	-0.6	2.1E-23

The zeta potential for colloids (ζ_c) and grains (ζ_g) were measured or estimated from the literature (Elimelech et al., 2000; Kuznar and Elimelech, 2007). Also included is the calculated resisting torque (T_{res}) according to Eq. (1).

Table 3 – The applied torque (T_{app}) for 1.1 and 3 μm colloids in several different sized capillary tubes (ranging in radius from 100 to 2.5 μm) at the minimum ($\Delta P/L_{ct} = 15696 \text{ N m}^{-3}$ for the 360 sand when $q = 0.1 \text{ cm min}^{-1}$) and maximum ($\Delta P/L_{ct} = 961478 \text{ N m}^{-3}$ for 150 sand when $q = 0.45 \text{ cm min}^{-1}$) value of the pressure gradient that was achieved in our column experiments according to Eqs. (3) and (4).

R (μm)	$\Delta P/L_{ct}$ —Minimum		$\Delta P/L_{ct}$ —Maximum	
	1.1 (μm)	3.0 (μm)	1.1 (μm)	3.0 (μm)
	T_{app} (Nm)	T_{app} (Nm)	T_{app} (Nm)	T_{app} (Nm)
2.5	7.8E-20	7.9E-19	4.9E-18	4.9E-17
5.0	1.8E-19	2.9E-18	1.1E-17	1.8E-16
10.0	3.9E-19	7.2E-18	2.4E-17	4.4E-16
50.0	2.1E-18	4.2E-17	1.3E-16	2.6E-15
100.0	4.3E-18	8.6E-17	2.6E-16	5.2E-15

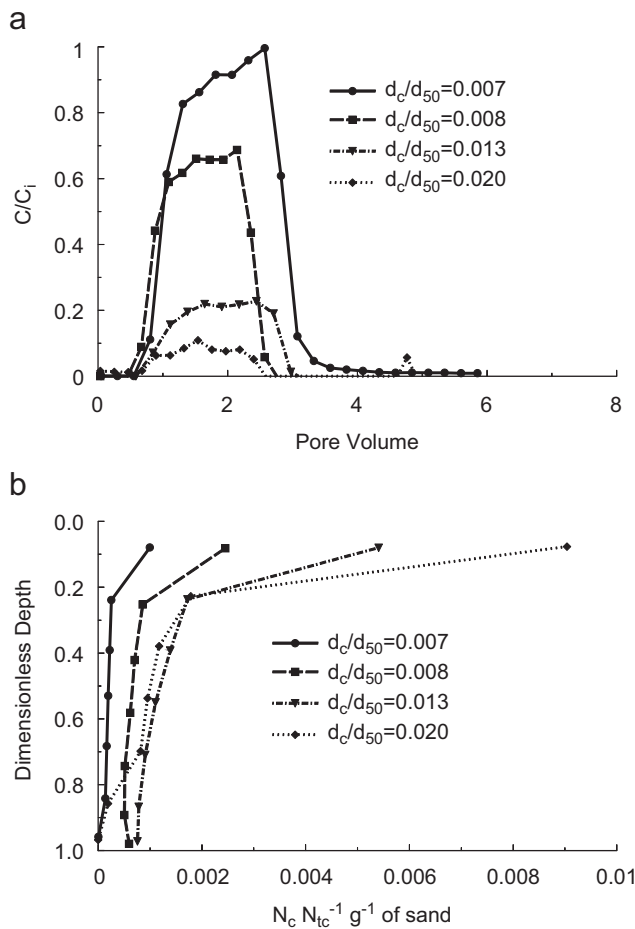


Fig. 1 – Effluent concentration curves (a) and deposition profiles (b) when the IS was 6 mM, the pH was 10, the ratio of the colloid diameter ($d_c = 1.1$ or 3 μm) to the median grain size ($d_{50} = 360, 240,$ or 150 μm) was varied from 0.007 to 0.02, and the Darcy velocity was approximately 0.1 cm min^{-1} .

and come to a region of the pore space where $T_{app} < T_{res}$ and/or there are physical limitations that are imposed on colloid transport by the size of the colloid and the pore space; i.e. a straining location adjacent to grain-grain contact points.

Fig. 1 presents effluent concentration curves (Fig. 1a) and deposition profiles (Fig. 1b) when the IS was 6 mM, the pH was 10, and the ratio of the colloid diameter (d_c) to the median grain size (d_{50}) was varied from 0.007 to 0.02. Effluent concentration curves are plotted herein with relative concentrations (C/C_i) on the y-axis and pore volume on the x-axis. Deposition profiles are plotted herein with the relative number (N_c/N_{tc} ; where N_c is the number of retained colloids and N_{tc} is the total number of colloids injected into the porous medium) per gram of dry sand on the x-axis and dimensionless distance from the column inlet (distance from inlet divided by the column length) on the y-axis. As noted previously, DLVO calculations presented in Table 2 indicate that deposition in the primary or secondary minimum was not expected for these colloids and porous media under these experimental conditions. As d_c/d_{50} increased, however, more deposition was observed, especially in the sand adjacent to the column inlet. These results are consistent with previous studies which observed enhanced colloid straining with increasing values of d_c/d_{50} (e.g., Bradford et al., 2003). Micromodel photos presented by Bradford et al. (2005) provide visual confirmation that similarly sized colloids were retained by straining in these Ottawa sands.

Fig. 2 presents effluent concentration curves for 1.1 μm modified carboxyl latex microspheres in 360 (Fig. 2a; $d_c/d_{50} = 0.003$), 240 (Fig. 2b; $d_c/d_{50} = 0.005$), and 150 (Fig. 2c; $d_c/d_{50} = 0.007$) μm Ottawa sand for a range of IS (6–106 mM) and a Darcy velocity of approximately 0.1 cm min^{-1} . Fig. 3 presents the corresponding deposition profiles for these systems. A systematic decrease in the peak effluent concentration and an increase in the colloid deposition is observed with increasing IS in Figs. 2 and 3. Many other researchers have reported a similar dependence of colloid transport on IS under unfavorable attachment conditions (e.g., Li et al., 2004; Tufenkji and Elimelech, 2004, 2005a). This has commonly been attributed to changes in the DLVO total interaction energy between colloids and collector grains. Specifically, at higher ionic strengths the energy barrier to deposition in the primary minimum decreases and the depth of the secondary minimum increases (see Table 2). Enhanced attachment with increasing IS has therefore been attributed to surface charge variability of the grain surfaces and colloids, and interactions associated with the secondary minimum (e.g., Tufenkji and Elimelech, 2004, 2005a).

Inspection of Fig. 3 reveals that most of the enhanced deposition with increasing IS occurs at the inlet of the column. This trend is similar to that seen in Fig. 1b for increasing d_c/d_{50} . Comparison of Figs. 3a–c reveal that the shape of the deposition profile is also highly dependent on the grain size of the sand. For a given IS, the deposition profiles tend to exhibit a more gradual change in retained concentration with depth for the coarser textured sand. Conversely, as the sand size is decreased the profiles tend to become more hyper-exponential for a given IS. Comparison with Fig. 2, as well as effluent mass balance information presented in Table 1, further indicates that the magnitude of colloid deposition depends on both the sand size and the IS. When

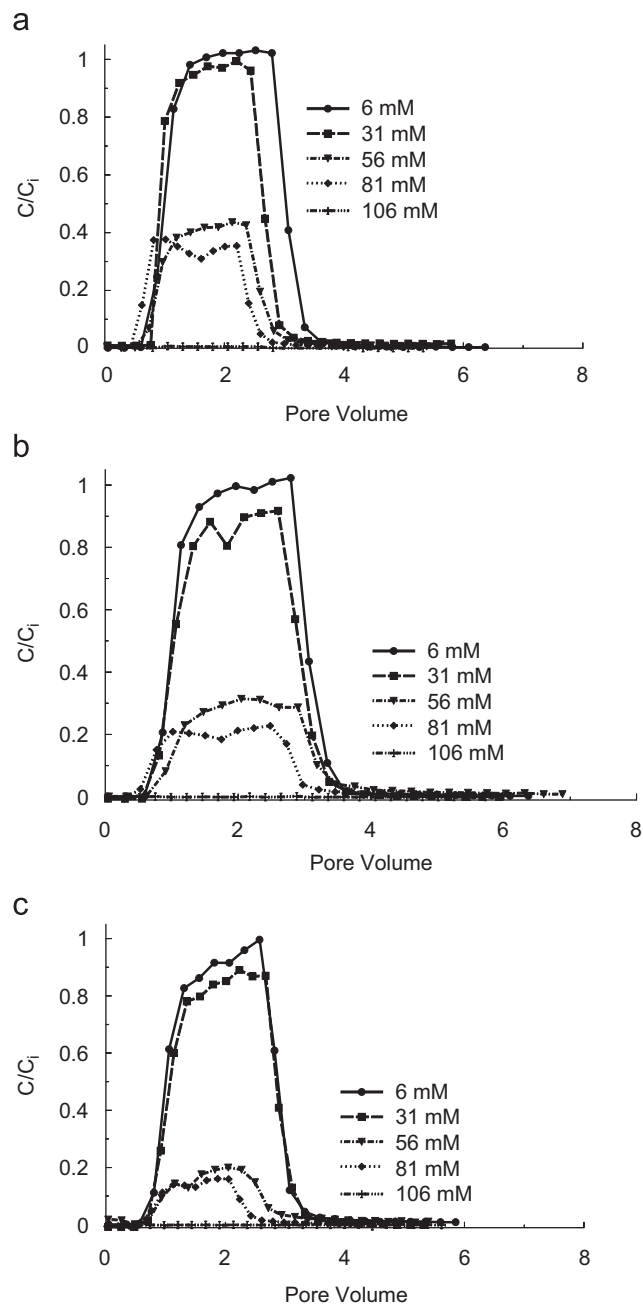


Fig. 2 – Effluent concentration curves for 1.1 μm modified carboxyl latex microspheres in 360 (a; $d_c/d_{50} = 0.003$), 240 (b; $d_c/d_{50} = 0.005$), and 150 (c; $d_c/d_{50} = 0.007$) μm Ottawa sand when the IS ranged from 6 to 106 mM and the Darcy velocity was approximately 0.1 cm min^{-1} .

the IS was 6 or 31 mM the amount of deposition was relatively insensitive to the grain size. Conversely, when the IS was 56 or 81 mM the role of grain size on deposition is much more pronounced; i.e. increasing with decreasing sand size. When the IS was 106 mM the role of grain size is only apparent by distinct differences in the shape of the deposition profiles (Fig. 3), because most of the colloids are retained in the sands. The above information provides evidence that the physical and chemical phenomena controlling deposition are inextricably related.

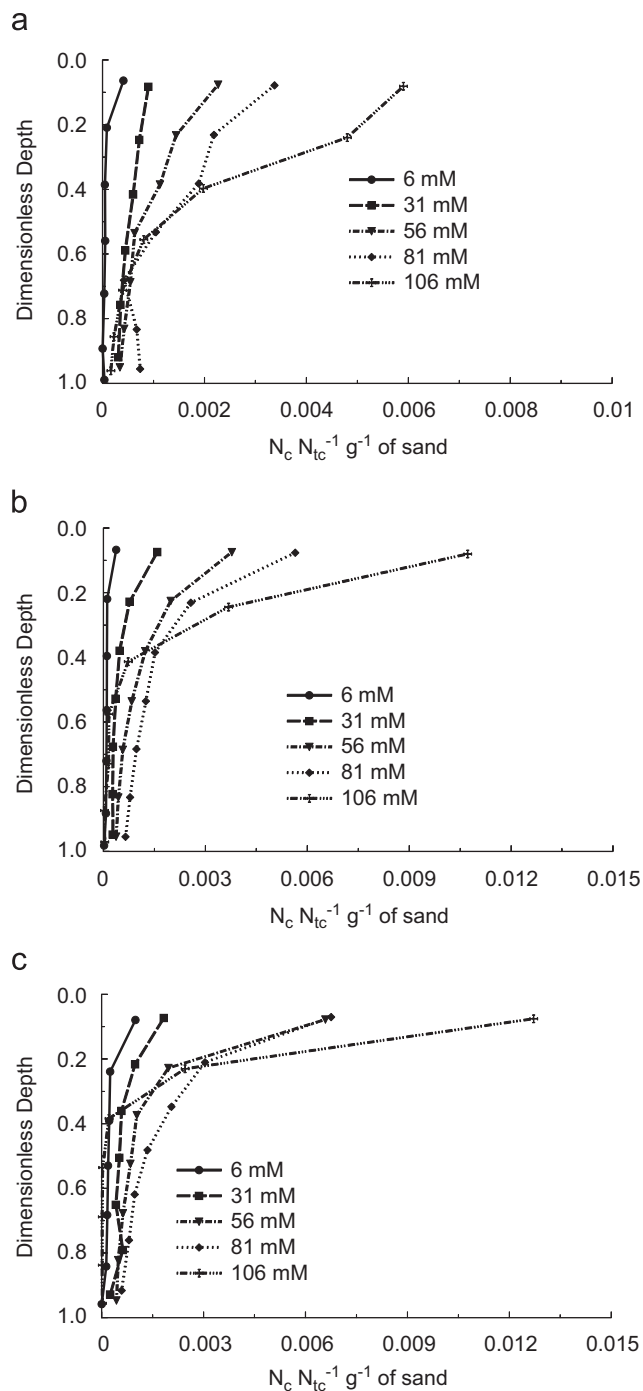


Fig. 3 – Deposition profiles for 1.1 μm modified carboxyl latex microspheres in 360 (a; $d_c/d_{50} = 0.003$), 240 (b; $d_c/d_{50} = 0.005$), and 150 (c; $d_c/d_{50} = 0.007$) μm Ottawa sand when the IS ranged from 6 to 106 mM and the Darcy water velocity was approximately 0.1 cm min^{-1} .

Additional experiments were conducted to better understand the relative roles of grain size and solution composition on colloid deposition. In these experiments the column was flushed with an additional 2.1–3.2 pore volumes of 6 mM solution before excavation of the sand and determination of the deposition profiles. Fig. 4 presents the measured effluent concentration curves (Fig. 4a) and deposition profiles (Fig. 4b)

for 1.1 μm colloid transport experiments conducted in 150, 240, and 360 μm Ottawa sand when the IS was initially 56 mM and then switched to 6 mM (referred to as 56/6 mM). Also included in this figure for reference is an 1.1 μm colloid transport experiment conducted in 150 μm sand when the IS was maintained at 6 mM. In all cases, the Darcy water velocity was approximately 0.2 cm min^{-1} . Fig. 5 presents similar information as in Fig. 4, however the experiments reported in Fig. 5 involved an initial IS of 106 mM before switching to 6 mM solution (referred to as 106/6 mM). Table 1 provides additional information about specific experimental conditions.

It is observed in Figs. 4a and 5a that a second peak in the effluent concentration curve occurred when the solution IS was changed from the higher value (56 or 106 mM) to 6 mM as a result of colloid release. This behavior has typically been ascribed to release of colloids associated with the solid surface via the secondary minimum (Franchi and O'Melia,

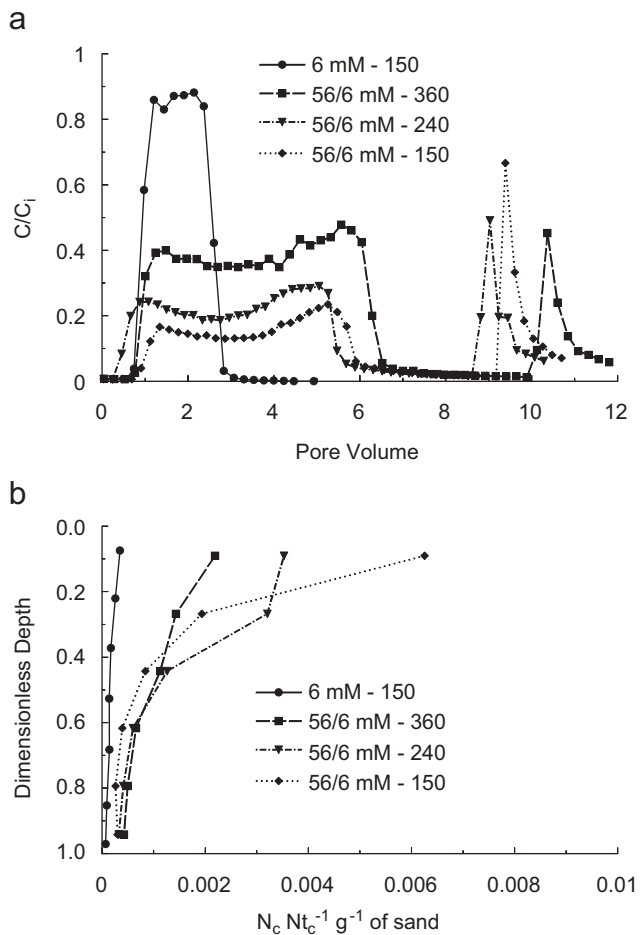


Fig. 4 – Effluent concentration curves (a) and deposition profiles (b) for 1.1 μm modified carboxyl latex microspheres in 150, 240, and 360 μm Ottawa sand when the Darcy water velocity was approximately 0.2 cm min^{-1} . In these experiments the column was flushed with colloid suspension and eluant at an IS of 56 mM for around the first 8–10 pore volumes and then switched to low IS solution of 6 mM for the final 2–3 pore volumes.

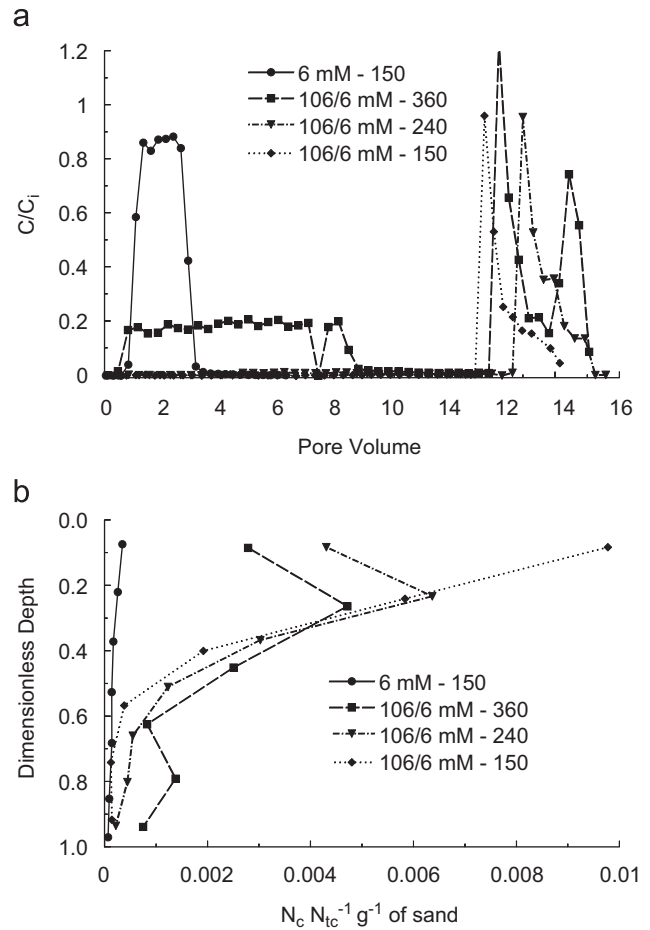


Fig. 5 – Effluent concentration curves (a) and deposition profiles (b) for 1.1 μm modified carboxyl latex microspheres in 150, 240, and 360 μm Ottawa sand when the Darcy water velocity was approximately 0.2 cm min^{-1} . In these experiments the column was flushed with colloid suspension and eluant at an IS of 106 mM for around the first 8–10 pore volumes and then switched to low IS solution of 6 mM for the final 2–3 pore volumes.

2003; Hahn and O'Melia, 2004; Hahn et al., 2004). Secondary minima association alone cannot explain the observed behavior. The first piece of evidence is that the corresponding deposition profile (Figs. 4b and 5b) are not exponential, even after a flushing step with an additional 2.1–3.2 pore volumes of 6 mM solution. Second, mass balance calculations indicate that the total amount of colloids recovered in the effluent only accounts for a small percentage of the injected colloid mass. For the 56/6 mM systems shown in Fig. 4a only 46%, 32%, and 25% of the injected colloids were recovered in the effluent for the 360, 240, and 150 μm sand, respectively. Similarly, for the 106/6 mM systems shown in Fig. 5a only 39%, 12%, and 11% of the injected colloids were recovered in the effluent for the 360, 240, and 150 μm sand, respectively. In contrast, effluent recovery for transport experiment conducted using only 6 mM solution and 150 μm sand was greater than 83% of the injected colloids (Table 1). Hence, adjustments in solution IS were observed to significantly increase

the total deposition in these sands, with enhanced deposition occurring in finer textured sand and for higher initial IS conditions.

Mass balance information further indicates that the amount of colloids recovered in the second “release” peak ($PV > 8$) shown in Figs. 4a and 5a accounted for only a small percentage of the injected colloids. For the 56/6 mM conditions shown in Fig. 4a only 5%, 6%, and 7% of the injected colloid mass was released in the second peak for the 360, 240, and 150 μm sands, respectively. For the 106/6 mM experiments shown in Fig. 5a only 19%, 11%, and 10% of the injected colloid mass was released in the second peak for the 360, 240, and 150 μm sands, respectively.

All of the above observations strongly indicate that the solution chemistry played an important role in colloid deposition and that this process was interrelated with pore structure. We postulate that straining and solution chemistry are coupled in the following ways. First, we believe that colloids may collide with grain surfaces via sedimentation, interception, and diffusion as assumed in traditional filtration theory. In the presence of an energy barrier to deposition in the primary minima, colloids that are weakly associated with the grain surface via the secondary minima can be translated along grain surfaces by hydrodynamic shear to regions of the pore space that are more favorable for deposition such as small pore spaces that are formed adjacent to grain-to-grain contacts. Deposition of colloids in these straining locations is expected to be greater than on other regions of the solid–water surface due to chemical and physical considerations. DLVO forces holding colloids in the smallest region of the pore space are greater than on a single solid–water interface due to the presence of multiple solid–water interfaces (Hoek and Agarwal, 2006). The fluid drag force is also decreased in the smallest region of the pore space because of lower fluid velocities (see Table 3). Finally, physical limitations that are imposed by the size of the colloid and pore, and/or by changes in pore surface topology are also expected to play a role in colloid retention.

Increasing the IS results in a greater depth of the secondary minimum (Table 2). Therefore, under unfavorable attachment conditions, increasing the solution IS may lead to greater numbers of colloids that are directed to small pore spaces where straining occurs. Once colloids are retained in the smallest region of the pore space, reduction of DLVO forces does not necessarily release these colloids because of physical limitations (size of colloid and pore) and reduced fluid drag in these locations.

3.2. Influence of hydrodynamics on colloid retention

As the water velocity increases the magnitudes of the lift and drag forces that act on colloids near solid surfaces will increase (Cushing and Lawler, 1998; Bergendahl and Grasso, 1998; Li et al., 2005), and the volume of low velocity (stagnant) regions is expected to decrease. All of these factors may inhibit straining of colloids in small pore spaces. It is therefore likely that the shape and magnitude of the deposition profiles for strained colloids will be very sensitive to flow rate. Fig. 6 presents effluent concentration curves for 1.1 μm colloids in 360 (Fig. 6a; $d_c/d_{50} = 0.003$), 240 (Fig. 6b; $d_c/d_{50} = 0.005$), and 150 (Fig. 6c; $d_c/d_{50} = 0.007$) μm sand when the IS was 56 mM and the Darcy velocity was approximately 0.1, 0.2, and 0.45 cm min^{-1} . Corresponding deposition profiles for these same systems are presented in Figs. 7a–c. For a given sand and IS = 56 mM the effluent concentration curves and deposition profiles were very similar when the velocity was

$d_{50} = 0.005$), and 150 (Fig. 6c; $d_c/d_{50} = 0.007$) μm sand when the IS was 56 mM and the Darcy velocity was approximately 0.1, 0.2, and 0.45 cm min^{-1} . Corresponding deposition profiles for these same systems are presented in Figs. 7a–c. For a given sand and IS = 56 mM the effluent concentration curves and deposition profiles were very similar when the velocity was

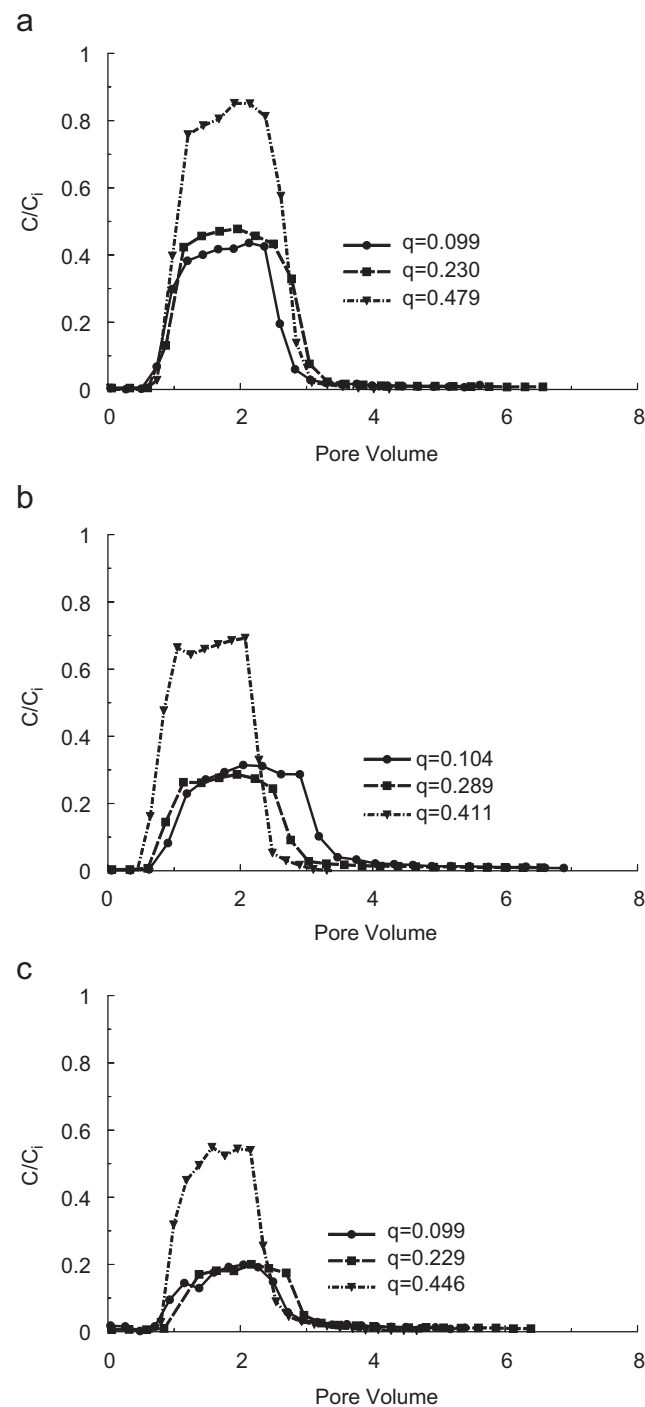


Fig. 6 – Effluent concentration curves for 1.1 μm colloids in 360 (a), 240 (b), and 150 (c) μm sand when the IS was 56 mM and the Darcy velocity was approximately 0.1, 0.2, and 0.45 cm min^{-1} .

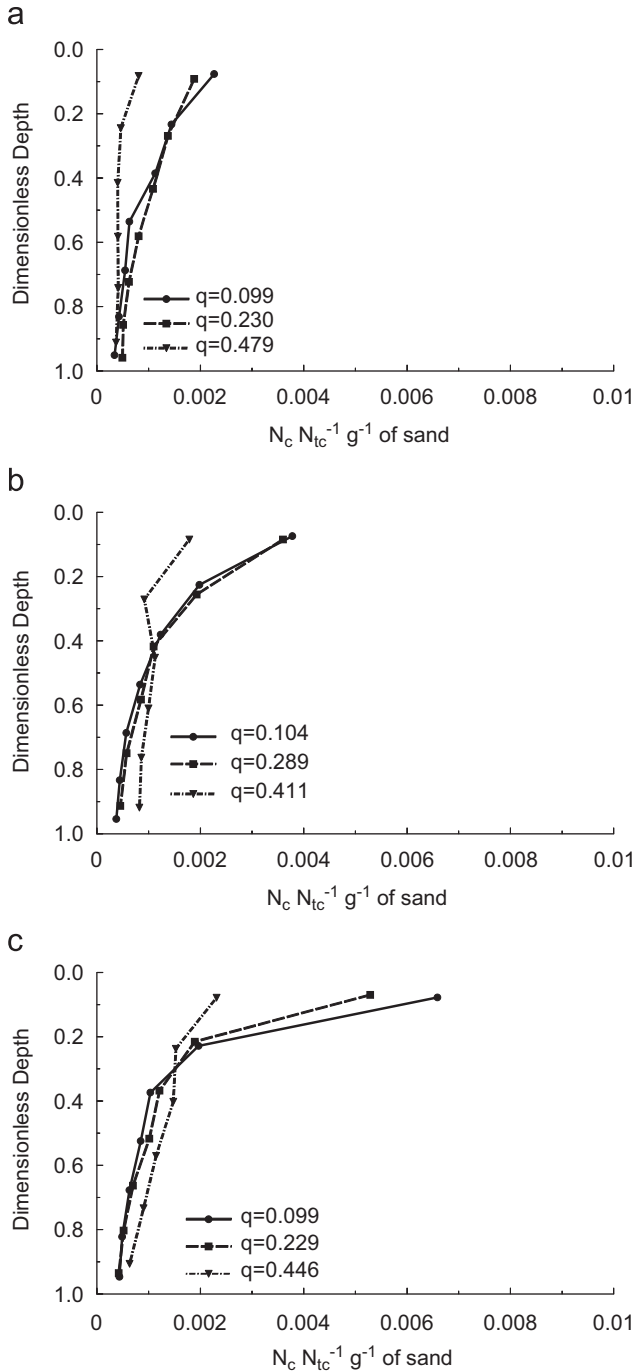


Fig. 7 – Deposition profiles for 1.1 μm colloids in 360 (a), 240 (b), and 150 (c) μm sand when the IS was 56 mM and the Darcy velocity was approximately 0.1, 0.2, and 0.45 cm min^{-1} .

0.1 and 0.2 cm min^{-1} . The influence of water velocity on the effluent concentration curves and deposition profiles was much more pronounced when the velocity was more than doubled to a value approaching 0.45 cm min^{-1} . In this case, the higher Darcy velocity produced an increase in the effluent concentration that was approximately 35% regardless of sand size. The highest Darcy velocity ($q = 0.45 \text{ cm min}^{-1}$) also produced a much more gradual change in the deposition

profiles with depth; i.e. the profiles were less hyper-exponential. In this case, we hypothesize that the fluid drag forces were sufficient to inhibit colloid retention in regions of the pore space that would otherwise retained colloids at the lower Darcy velocities (0.1 and 0.2 cm min^{-1}).

In order to further compare the role of hydrodynamics on colloid straining, additional transport experiments were conducted with 3 μm colloids in 360 ($d_c/d_{50} = 0.008$), 240 ($d_c/d_{50} = 0.013$), and 150 ($d_c/d_{50} = 0.02$) μm sand when the IS was 6 mM and the Darcy velocity was about 0.1 (Fig. 1) and 0.45 (Fig. 8) cm min^{-1} . Comparison of Figs. 1 (0.1 cm min^{-1}) and 8 (0.45 cm min^{-1}) indicate that increasing the flow rate produced greater deposition, especially for the coarser textured 360 μm sand. The effluent concentration after around one pore volume at the higher flow rate (0.45 cm min^{-1}) also tended to decrease as injection of colloids continued. This time-dependent deposition behavior has typically been ascribed to ripening; i.e. favorable colloid–colloid interactions during attachment. Recall that the experimental conditions were designed to minimize colloid attachment in this instance, so as to better deduce mechanisms of colloid straining. Hence, the data in Fig. 8 suggests that increasing the flow rate may lead not only to colloid retention in pores

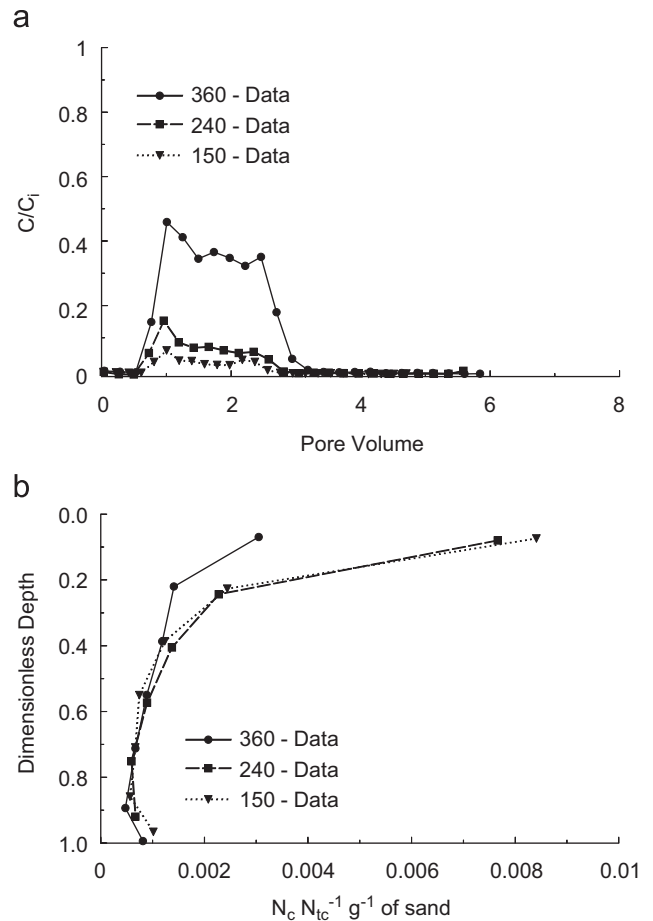


Fig. 8 – Effluent concentration curves (a) and deposition profiles (b) for 3 μm colloids in 360, 240, and 150 μm sand when the IS was 6 mM and the Darcy velocity was approximately 0.45 cm min^{-1} .

and at grain–grain junctions, but that the deposition morphology may also influence subsequent retention in these locations. One potential explanation is that retained colloids in a pore constriction reduce the effective size of the pore and therefore increase subsequent straining at this location. A second hypothesis is that colloid–colloid interactions are enhanced in pores because the number of collisions in small pores has the potential to drastically increase relative to that in bulk solution. Additional research is needed to further test these hypotheses, but is beyond the scope of this work.

Comparison of Figs. 1, 6–8 indicates that increasing the Darcy velocity from 0.1 to 0.45 cm min⁻¹ had an opposite effect on colloid deposition for the 3 μm colloids in 6 mM solution (increasing extent of deposition) than the 1.1 μm colloids in 56 mM solution (decreasing deposition). Differences in the influence of velocity on the deposition behavior for these two colloids is likely a result of the deposition morphology in the small pore spaces and the fluid drag forces. Size limitations in small pores are also expected to be more pronounced for the 3 than 1.1 μm colloids, and release of these colloids by fluid drag forces is therefore believed to be more difficult. Conversely, for the 1.1 μm colloids in 56 mM solution we hypothesized that increasing the water velocity and associated fluid drag were sufficient to inhibit colloid retention in small pores.

4. Conclusions

Experimental and theoretical studies were undertaken to determine the role of solution chemistry and hydrodynamics on straining under unfavorable attachment conditions. To better isolate the effects of straining on colloid retention, the experimental conditions were selected to minimize the potential for colloid attachment (solution pH of 10, simple aqueous chemistries, quartz sands, and highly negatively charged colloids that were hydrophilic). DLVO calculations, analysis of torques, and mass balance information confirm our assumption that attachment did not play a dominant role in colloid deposition. Experimental data and analysis of torques indicate a complex interaction of hydrodynamics, solution chemistry, colloid size, and pore structure (grain size) on colloid transport and straining. Specific findings are highlighted below.

- Straining increases in magnitude with increasing IS due to an increased force and number of colloids that are funneled to and retained in small pores formed adjacent to grain–grain junctions.
- Straining can play a very significant role in colloid deposition when d_c/d_{50} is as low as 0.003.
- Reduction in solution IS will not release colloids that are retained in straining locations.
- The shape of the colloid deposition profile is highly sensitive to the physical (colloid and grain size, and system hydrodynamics) and chemical (solution IS and pH) properties of a system due to the interrelation of these parameters on straining.
- Increasing the flow rate of a system tends to decrease the amount of straining as a result of the increased fluid drag

force that acts on colloids in pores, but the magnitude of this effect is expected to be highly dependent on the solution chemistry and the size of the colloid and sand.

This information is believed to be essential for predicting colloid transport and fate in many natural environments.

Acknowledgments

This research was supported by the 206 Manure and Byproduct Utilization Project of the USDA-ARS and in part by grants from NRI and EPA (NRI #:2006-02541 and EPA IAG # DW-12-92189901-0). Although this work has been supported by the USDA and the EPA, it has not been subjected to Agency review and therefore does not necessarily reflect the views of the Agency, and no official endorsement should be inferred. Similarly, mention of trade names and company names in this manuscript does not imply any endorsement or preferential treatment by the USDA or EPA. We would also like to acknowledge helpful discussions with William P. Johnson on the role of solution chemistry and hydrodynamics on straining deposition, and the efforts of Yadata F. Tadassa and Michael Troung in helping to conduct the column studies.

REFERENCES

- Albinger, O., Biesemeyer, B.K., Arnold, R.G., Logan, B.E., 1994. Effect of bacterial heterogeneity on adhesion to uniform collectors by monoclonal populations. *FEMS Microbiol. Lett.* 124 (3), 321–326.
- Bergendahl, J., Grasso, D., 1998. Colloid generation during batch leaching tests: mechanics of disaggregation. *Colloids Surf. A Physicochem. Eng. Aspects* 135, 193–205.
- Bergendahl, J., Grasso, D., 1999. Prediction of colloid detachment in a model porous media: thermodynamics. *AIChE J.* 45 (3), 475–484.
- Bergendahl, J., Grasso, D., 2000. Prediction of colloid detachment in a model porous media: hydrodynamics. *Chem. Eng. Sci.* 55, 1523–1532.
- Bolster, C.H., Mills, A.L., Hornberger, G.M., Herman, J.S., 1999. Spatial distribution of deposited bacteria following miscible displacement experiments in intact cores. *Water Resour. Res.* 35, 1797–1807.
- Bradford, S.A., Abriola, L.M., 2001. Dissolution of residual tetrachloroethylene in fractional wettability porous media: incorporation of interfacial area estimates. *Water Resour. Res.* 37, 1183–1195.
- Bradford, S.A., Bettahar, M., 2005. Straining, attachment, and detachment, of *Cryptosporidium* oocysts in saturated porous media. *J. Environ. Qual.* 34, 469–478.
- Bradford, S.A., Yates, S.R., Bettahar, M., Simunek, J., 2002. Physical factors affecting the transport and fate of colloids in saturated porous media. *Water Resour. Res.* 38, Art. no. 1327, doi:10.1029/2002WR001340.
- Bradford, S.A., Simunek, J., Bettahar, M., van Genuchten, M.T., Yates, S.R., 2003. Modeling colloid attachment, straining, and exclusion in saturated porous media. *Environ. Sci. Technol.* 37, 2242–2250.
- Bradford, S.A., Bettahar, M., Simunek, J., van Genuchten, M.T., 2004. Straining and attachment of colloids in physically heterogeneous porous media. *Vadose Zone J.* 3, 384–394.

- Bradford, S.A., Simunek, J., Bettahar, M., Tadassa, Y.F., van Genuchten, M.T., Yates, S.R., 2005. Straining of colloids at textural interfaces. *Water Resour. Res.* 41, Art. no. W10404, doi:10.1029/2004WR003675.
- Bradford, S.A., Bettahar, M., 2006. Concentration dependent colloid transport in saturated porous media. *J. Contam. Hydrol.* 82, 99–117.
- Bradford, S.A., Tadassa, Y.F., Pachepsky, Y.A., 2006a. Transport of *Giardia* and manure suspensions in saturated porous media. *J. Environ. Qual.* 35, 749–757.
- Bradford, S.A., Simunek, J., Walker, S.L., 2006b. Transport and straining of *E. coli* O157:H7 in saturated porous media. *Water Resour. Res.* 42, W12S12.
- Bradford, S.A., Tadassa, Y.F., Jin, Y., 2006c. Transport of coliphage in the presence and absence of manure suspension. *J. Environ. Qual.* 35, 1692–1701.
- Bradford, S.A., Simunek, J., Bettahar, M., van Genuchten, M.T., Yates, S.R., 2006d. Significance of straining in colloid deposition: evidence and implications. *Water Resour. Res.* 42, W12S15.
- Brow, C.N., Li, X., Ricka, J., Johnson, W.P., 2005. Comparison of microsphere deposition in porous media versus simple shear systems. *Colloids Surf. A Physicochem. Eng. Aspects* 252, 125–136.
- Camesano, T.A., Logan, B.E., 1998. Influence of fluid velocity and cell concentration on the transport of motile and nonmotile bacteria in porous media. *Environ. Sci. Technol.* 32 (11), 1699–1708.
- Compere, F., Porel, G., Delay, F., 2001. Transport and retention of clay particles in saturated porous media: influence of ionic strength and pore velocity. *J. Contam. Hydrol.* 49, 1–21.
- Cherrey, K.D., Flury, M., Harsh, J.B., 2003. Nitrate and colloid transport through coarse Hanford sediments under steady state, variably saturated flow. *Water Resour. Res.* 39, 1165.
- Cushing, R.S., Lawler, D.F., 1998. Depth filtration: fundamental investigation through three-dimensional trajectory analysis. *Environ. Sci. Technol.* 32, 3793–3801.
- Derjaguin, B.V., Landau, L.D., 1941. Theory of the stability of strongly charged lyophobic sols and of the adhesion of strongly charged particles in solutions of electrolytes. *Acta Physicochim. USSR* 14, 733–762.
- Elimelech, M., Nagai, M., Ko, C.H., Ryan, J.N., 2000. Relative insignificance of mineral grain zeta potential to colloid transport in geochemically heterogeneous porous media. *Environ. Sci. Technol.* 34, 2143–2148.
- Franchi, A., O'Melia, C.R., 2003. Effects of natural organic matter and solution chemistry on the deposition and reentrainment of colloids in porous media. *Environ. Sci. Technol.* 37 (6), 1122–1129.
- Foppen, J.W.A., Mporokoso, A., Schijven, J.F., 2005. Determining straining of *Escherichia coli* from breakthrough curves. *J. Contam. Hydrol.* 76, 191–210.
- Ginn, T.R., Wood, B.D., Nelson, K.E., Schiebe, T.D., Murphy, E.M., Clement, T.P., 2002. Processes in microbial transport in the natural subsurface. *Adv. Water Res.* 25, 1017–1042.
- Gregory, J., 1981. Approximate expression for retarded van der Waals interaction. *J. Colloid Interface Sci.* 83, 138–145.
- Hahn, M.W., O'Melia, C.R., 2004. Deposition and reentrainment of Brownian particles in porous media under unfavorable chemical conditions: some concepts and applications. *Environ. Sci. Technol.* 38 (1), 210–220.
- Hahn, M.W., Abadzic, D., O'Melia, C.R., 2004. Aquasols: on the role of secondary minima. *Environ. Sci. Technol.* 38, 5915–5924.
- Harvey, R.W., Harms, H., 2002. Transport of microorganisms in the terrestrial subsurface: in situ and laboratory methods. In: Hurst, C.J., Knudsen, G.R., McInerney, M.J., Stetzenback, L.D., Crawford, R.L. (Eds.), *Manual of Environmental Microbiology*, second ed. ASM Press, Washington, DC, pp. 753–776.
- Hoek, E.M.V., Agarwal, G.K., 2006. Extended DLVO interactions between spherical particles and rough surfaces. *J. Colloid Interface Sci.* 298, 50–58.
- Hogg, R., Healy, T.W., Fuerstenau, D.W., 1966. Mutual coagulation of colloidal dispersions. *Trans. Faraday Soc.* 62, 1638–1651.
- Israelachvili, J.N., 1992. *Intermolecular and Surface Forces*, second ed. Academic Press, London, England.
- Jin, Y., Flury, M., 2002. Fate and transport of viruses in porous media. *Adv. Agron.* 77, 39–102.
- Jury, W.A., Gardner, W.R., Gardner, W.H., 1991. *Soil Physics*, fifth ed. Wiley, New York.
- Kretzschmar, R., Barmettler, K., Grolimun, D., Yan, Y.D., Borkovec, M., Sticher, H., 1997. Experimental determination of colloid deposition rates and collision efficiencies in natural porous media. *Water Resour. Res.* 33 (5), 1129–1137.
- Kuznar, Z.A., Elimelech, M., 2007. Direct microscopic observation of particle deposition in porous media: role of the secondary energy minimum. *Colloid Surf. A: Physicochem. Eng. Aspects* 294, 156–162.
- Li, X., Johnson, W.P., 2005. Nonmonotonic variations in deposition rate coefficients of microspheres in porous media under unfavorable deposition conditions. *Environ. Sci. Technol.* 39, 1658–1665.
- Li, X., Scheibe, T.D., Johnson, W.P., 2004. Apparent decreases in colloid deposition rate coefficient with distance of transport under unfavorable deposition conditions: a general phenomenon. *Environ. Sci. Technol.* 38 (21), 5616–5625.
- Li, X., Zhang, P., Lin, C.L., Johnson, W.P., 2005. Role of hydrodynamic drag on microsphere deposition and re-entrainment in porous media under unfavorable conditions. *Environ. Sci. Technol.* 39, 4012–4020.
- Li, X., Lin, C.L., Miller, J.D., Johnson, W.P., 2006a. Pore-scale observation of microsphere deposition at grain-to-grain contacts over assemblage-scale porous media domains using X-ray microtomography. *Environ. Sci. Technol.* 40, 3762–3768.
- Li, X., Lin, C.L., Miller, J.D., Johnson, W.P., 2006b. Role of grain-to-grain contacts on profiles of retained colloids in porous media in the presence of an energy barrier to deposition. *Environ. Sci. Technol.* 40, 3769–3774.
- Redman, J.A., Grant, S.B., Olson, T.M., Estes, M.K., 2001. Pathogen filtration, heterogeneity, and the potable reuse of wastewater. *Environ. Sci. Technol.* 35 (9), 1798–1805.
- Redman, J.A., Walker, S.L., Elimelech, M., 2004. Bacterial adhesion and transport in porous media: role of the secondary energy minimum. *Environ. Sci. Technol.* 38, 1777–1785.
- Schijven, J.K., Hassanizadeh, S.M., 2000. Removal of viruses by soil passage: overview of modeling, processes, and parameters. *Crit. Rev. Environ. Sci. Technol.* 30, 49–127.
- Tan, Y., Cannon, J.T., Baveye, P., Alexander, M., 1994. Transport of bacteria in an aquifer sand—experiments and model simulations. *Water Resour. Res.* 30, 3243–3252.
- Tipping, E., 1981. The adsorption of aquatic humic substances by iron oxides. *Geochimica et Cosmochimica Acta* 45, 191–199.
- Tong, M., Li, X., Brow, C.N., Johnson, W.P., 2005. Detachment-influenced transport of an adhesion-deficient bacterial strain within water-reactive porous media. *Environ. Sci. Technol.* 39, 2500–2508.
- Torkzaban, S., Bradford, S.A., van Genuchten, M.T., Walker, S.L., 2006. Colloid transport in unsaturated porous media: the role of water content and ionic strength on particle straining. *J. Contam. Hydrol.*, submitted.
- Tufenkji, N., Elimelech, M., 2004. Deviation from the classical colloid filtration theory in the presence of repulsive DLVO interactions. *Langmuir* 20, 10818–10828.
- Tufenkji, N., Elimelech, M., 2005a. Breakdown of colloid filtration theory: role of the secondary energy minimum and surface charge heterogeneities. *Langmuir* 21, 841–852.

- Tufenkji, N., Elimelech, M., 2005b. Spatial distributions of *Cryptosporidium* oocysts in porous media: evidence for dual mode deposition. *Environ. Sci. Technol.* 39, 3620–3629.
- Tufenkji, N., Redman, J.A., Elimelech, M., 2003. Interpreting deposition patterns of microbial particles in laboratory-scale column experiments. *Environ. Sci. Technol.* 37 (3), 616–623.
- Tufenkji, N., Miller, G.F., Ryan, J.N., Harvey, R.W., Elimelech, M., 2004. Transport of *Cryptosporidium* oocysts in porous media: role of straining and physicochemical filtration. *Environ. Sci. Technol.* 38, 5932–5938.
- Verwey, E.J.W., Overbeek, J.T.G., 1948. *Theory of the Stability of Lyophobic Colloids*. Elsevier, Amsterdam.
- Walker, S.L., Redman, J.A., Elimelech, M., 2004. Role of cell surface lipopolysaccharides in *E. coli* K12 adhesion and transport. *Langmuir* 20, 7736–7746.
- Wang, D.S., Gerba, C.P., Lance, J.C., 1981. Effect of soil permeability on virus removal through soil. *Appl. Environ. Microbiol.* 42, 83–88.
- Yao, K.M., Habibian, M.T., O'Melia, C.R., 1971. Water and waste water filtration—concepts and applications. *Environ. Sci. Technol.* 5, 1105–1112.